J Mater Sci (2010) 45:5988–5992
DOI 10.1007/s10853-010-4802-z

LETTER

Micromechanically derived lowest threshold stress intensity factor for macroscopic stress-corrosion cracking in unidirectional GFRP composites

H. Sekine · P. W. R. Beaumont

Received: 5 March 2010 / Accepted: 27 July 2010 / Published online: 13 August 2010

Observation by scanning electron microscopy of a typical fracture surface in glass fiber-reinforced polymer (GFRP) composites shows that the fracture surface of each fiber is characterized by a mirror region surrounded by a hackle region. This indicates a two-stage fracture process: (1) a "slow" (meaning time-dependent) fracture of a portion of the glass fiber is followed by (2) a "fast" unstable fracture across the remainder of the glass fiber.

On the premise that the time-dependent failure of GFRP composites in acid environments is controlled by the initiation and slow growth of a crack from a pre-existing inherent surface flaw in a glass fiber, a micromechanical model of stress-corrosion crack growth (sometimes called the Sekine–Miyanaga–Beaumont model) was constructed [1–3]. Using this model, an equation was derived for the macroscopic crack growth rate as a function of the apparent crack tip stress intensity factor for the mode I. If tougher and more ductile matrices are used, there exists a lowest threshold value of the stress intensity factor. By assuming that the polymeric fibrils of matrix or ligaments stretched between the crack surfaces behave according to an ideal cohesive force model, i.e., the Dugdale model [4], the lowest threshold stress intensity factor was given in an explicit form [3]. However, the examination in the case of a more general cohesive force model, i.e., the Barenblatt model [5], has been left until now, although this examination will give a physically definite description of the lowest threshold stress intensity factor. We begin this examination with a brief review of our previous article [3].

In bulk glass, the stable crack growth rate due to stress-corrosion cracking $\mathrm{d}a/\mathrm{d}t$ can be given by

$$\frac{\mathrm{d}a}{\mathrm{d}t} = v \exp\left(-\frac{\Delta Q - \alpha K_{\mathrm{I}}}{RT}\right). \tag{1}$$

In this Arrhenius equation, ΔQ is the activation energy of the chemically activated process, K_{I} is the crack tip stress intensity factor for the mode I, R is the gas constant, T is absolute temperature, and v and α are empirical constants.

In our micromechanical model, the shape of the edge of stress-corrosion crack in a single glass fiber is represented as a circular arc of radius r, which is equal to the fiber radius r_{f} (Fig. 1). Then, the average crack growth rate can be written from Eq. 1 as

$$\frac{1}{2r_{\mathrm{f}}\theta}\frac{\mathrm{d}Y}{\mathrm{d}t} = v \exp\left(-\frac{\Delta Q - \alpha K_{\mathrm{I}}}{RT}\right), \tag{2}$$

where Y is the area of the stress-corrosion crack in the single glass fiber, θ is half the angle which is made by two fiber radii on the ends of the circular crack edge, and t is time. In Eq. 2, K_{I} should be interpreted as the average value of the crack tip stress intensity factor for the mode I along the entire crack edge. Since the crack tip stress intensity factor is constant, more or less, along the larger central portion of the circular crack edge, K_{I} can be represented by the crack tip stress intensity factor at the maximum depth of the stress-corrosion crack as follows:

$$K_{\mathrm{I}} = \sigma_{\mathrm{f}} F(\theta)\sqrt{2\pi r_{\mathrm{f}}}, \tag{3}$$

where σ_{f} is the axial tensile stress acting on the glass fiber and the geometrical function $F(\theta)$ can be seen in [3].

Figure 2a shows the schematic of actual aligned glass fibers and the edges of macroscopic stress-corrosion crack in

H. Sekine (✉)
Tohoku University, 6-6-01 Aoba-yama,
Aoba-ku, Sendai 980-8579, Japan
e-mail: sekine@plum.mech.tohoku.ac.jp

P. W. R. Beaumont
Department of Engineering, University of Cambridge,
Trumpington Street, Cambridge CB2 1PZ, UK

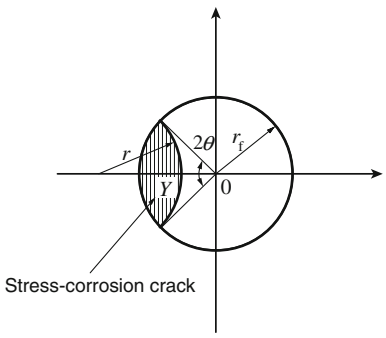

Fig. 1 Stress-corrosion crack in a single glass fiber

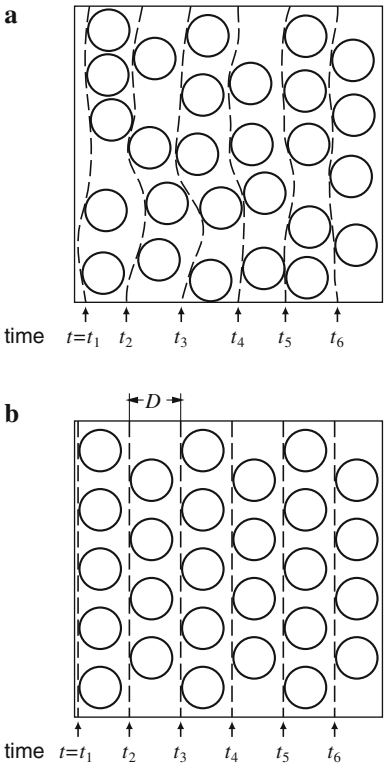

Fig. 2 **a** Schematic of actual aligned glass fibers and the edges of macroscopic stress-corrosion crack, **b** glass fibers distributed in a doubly periodic face-centered hexagonal array and straight edges of macroscopic stress-corrosion crack. The edges are indicated by broken lines

unidirectional GFRP composites. In this study, the arrangement of the glass fibers is ideally modeled as a doubly periodic face-centered hexagonal array illustrated in Fig. 2b, and the shape of the edges of macroscopic stress-corrosion crack in the matrix is assumed by a straight line. Then, the spacing D between the neighboring rows of glass fibers is

$$D = \sqrt{\frac{3^{1/2}\pi}{2V_{\mathrm{f}}}} r_{\mathrm{f}}, \tag{4}$$

where V_{f} is the volume fraction of glass fiber.

The unidirectional GFRP composite is macroscopically orthotropic. From the results [6] of linear elastic fracture mechanics of orthotropic elastic solids, the macroscopic tensile stress σ_y in front of the macroscopic stress-corrosion crack tip is

$$\sigma_y = \frac{K_{\mathrm{I}}^*}{\sqrt{2\pi x}}, \tag{5}$$

where K_{I}^* is the apparent crack tip stress intensity factor for the mode I and x is the rectangular coordinate whose origin is located at the macroscopic stress-corrosion crack tip (Fig. 3). Arguing that the average macroscopic tensile stress over a small distance D in front of the macroscopic stress-corrosion crack tip is shared between the glass fiber and matrix according to a rule of mixtures, we can obtain the relationship between the axial tensile stress acting on the glass fiber in front of the macroscopic stress-corrosion crack tip and the apparent crack tip stress intensity factor, as follows [3]:

$$\sigma_{\mathrm{f}} = \beta K_{\mathrm{I}}^* \tag{6}$$

where

$$\beta = \frac{E_{\mathrm{f}}}{V_{\mathrm{f}}E_{\mathrm{f}} + V_{\mathrm{m}}E_{\mathrm{m}}}\sqrt{\frac{2}{\pi D}}. \tag{7}$$

Here, E_{f} and E_{m} are the Young's moduli of glass fiber and matrix, respectively, and V_{m} $(= 1 - V_{\mathrm{f}})$ is the volume fraction of matrix.

Meanwhile, from a geometrical consideration of the area of the stress-corrosion crack in the single glass fiber, we obtain

$$\frac{\mathrm{d}Y}{\mathrm{d}t} = 4r_{\mathrm{f}}^2 \sin^2\theta \frac{\mathrm{d}\theta}{\mathrm{d}t}. \tag{8}$$

By substituting Eq. 8 into Eq. 2 and combining Eqs. 3 and 6, it follows that

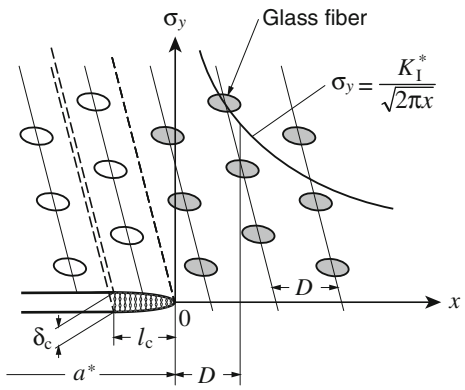

Fig. 3 Macroscopic tensile stress distribution in front of the macroscopic stress-corrosion crack tip

$$dt = \frac{2r_f}{vk}\frac{\sin^2\theta}{\theta}\exp\left(-\frac{\alpha\beta F(\theta)\sqrt{2\pi r_f}}{RT}K_I^*\right)d\theta, \quad (9)$$

where $k = \exp(-\Delta Q/RT)$. The time required for the slow crack growth stage of the stress-corrosion crack in the single glass fiber, t_F, is obtained by integrating Eq. 9, i.e.,

$$t_F = \frac{2r_f}{vk}\int_{\theta_0}^{\theta_F}\frac{\sin^2\theta}{\theta}\exp\left(-\frac{\alpha\beta F(\theta)\sqrt{2\pi r_f}}{RT}K_I^*\right)d\theta, \quad (10)$$

where θ_0 is half the angle made by two fiber radii on the ends of the edge of pre-existing inherent surface flaw and θ_F is the critical value at unstable fracture of the glass fiber. The above expression can be approximately written in the form [2]:

$$t_F \approx \frac{4D}{1.58\varsigma\mu K_I^*}\left(\frac{1}{1.58\mu K_I^*}+\frac{\theta_0}{2}\right)\exp\left(-0.79\mu\theta_0 K_I^*\right), \quad (11)$$

where

$$\varsigma = \frac{vkD}{2r_f}, \quad \mu = \frac{\alpha\beta\sqrt{2\pi r_f}}{RT}. \quad (12)$$

Now the time required for unstable fractures of the glass fiber and matrix is much shorter than the time t_F given by Eq. 10. It follows, therefore, that the macroscopic crack growth rate da^*/dt is approximately given by

$$\frac{da^*}{dt} = \frac{D}{t_F}. \quad (13)$$

By substituting Eq. 11 into Eq. 13, the macroscopic crack growth rate da^*/dt can be written as a function of K_I^* in the form:

$$\frac{da^*}{dt} = 1.25\varsigma\mu^2 K_I^{*2}\left(\frac{1}{2+1.58\mu\theta_0 K_I^*}\right)\exp\left(0.79\mu\theta_0 K_I^*\right). \quad (14)$$

If the matrix is made of a ductile polymer, matrix bridging shown schematically in Fig. 3 may occur in the crack wake. Then, the bridged crack has a reduced apparent crack tip stress intensity factor, and it follows that

$$K_I^* = K_{Ia}^* + K_{Ib}^*, \quad (15)$$

where K_{Ia}^* and K_{Ib}^* are the apparent crack tip stress intensity factors due to the remote applied stress and matrix bridging, respectively.

In this study, we assume that the polymeric fibrils of matrix stretched between the crack surfaces behave according to a Barenblatt cohesive force model [5] as depicted in Fig. 4, where σ is the cohesive stress, δ is the opening displacement, and δ_c is the maximum value of the opening displacement. It is worthwhile noting that δ_c corresponds to the crack opening displacement at the end of the fully developed bridging zone of length l_c, as shown in Fig. 3. When l_c is extremely small compared to the crack length, the relationship between δ_c and l_c is

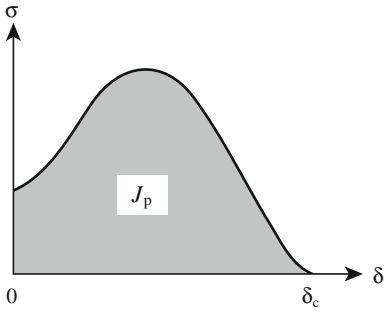

Fig. 4 Barenblatt cohesive force model of polymeric fibrils

$$\delta_c = 4\Phi K_I^*\sqrt{\frac{l_c}{2\pi}}. \quad (16)$$

For the plane strain problem of orthotropic elastic solids, Φ is written as

$$\Phi = \sqrt{b_{22}\{2(b_{11}b_{22})^{1/2}+2b_{12}+b_{66}\}} \quad (17)$$

where b_{11}, b_{12}, b_{22}, and b_{66} can be expressed in terms of the elastic moduli of unidirectional GFRP composite, as follows:

$$b_{11} = \frac{1-v_{TT}^2}{E_T}, \quad b_{12} = -\frac{v_{LT}(1+v_{TT})}{E_L}, \quad b_{22} = \frac{1-E_T v_{LT}^2/E_L}{E_L}, \quad b_{66} = \frac{1}{G_{LT}}. \quad (18)$$

Here, E_L and E_T are the Young's moduli of unidirectional GFRP composite in the longitudinal and transverse directions, respectively; v_{LT} and v_{TT} are the Poisson's ratios for transverse strain under applied loading in the longitudinal and transverse directions, respectively; and G_{LT} is the shear modulus.

For an extremely small bridging zone compared to the crack length, the apparent crack tip stress intensity factor due to the matrix bridging is written using the solution [6] for a concentrated force on the crack surface in orthotropic elastic solids, as

$$K_{Ib}^* = -2V_m\int_{-l_c}^{0}\frac{\sigma}{\sqrt{-2\pi x}}dx. \quad (19)$$

By transforming the variable x into δ using the relationship between δ and x, i.e.,

$$\delta = 4\Phi K_I^*\sqrt{-\frac{x}{2\pi}} \quad (20)$$

and combining Eq. 16, Eq. 19 leads to

$$K_{Ib}^* = -\frac{V_m J_p}{\Phi K_I^*}, \quad (21)$$

where J_p is the fracture energy of polymeric fibrils, which is defined by $J_p = \int_0^{\delta_c} \sigma d\delta$.

Substituting Eq. 21 into Eq. 15, we obtain

$$K_I^{*2} - K_{Ia}^* K_I^* + V_m J_p/\Phi = 0. \quad (22)$$

The solution of this equation for K_I^* is

$$K_I^* = \frac{K_{Ia}^* + \sqrt{K_{Ia}^{*2} - 4V_m J_p/\Phi}}{2} \quad (23)$$

where

$$K_{Ia}^* \geq 2\sqrt{V_m J_p/\Phi}\,. \quad (24)$$

Note that $K_I^* = (K_{Ia}^* - \sqrt{K_{Ia}^{*2} - 4V_m J_p/\Phi})/2$ is the incompatible solution of Eq. 22.

Substituting Eq. 23 into Eq. 14, we can obtain the macroscopic crack growth rate da^*/dt as a function of the apparent crack tip stress intensity factor due to the remote applied stress K_{Ia}^*. Figure 5 shows a logarithmic plot of da^*/dt versus K_{Ia}^* for selected values of θ_0 and J_p. Values of ς, μ, V_m, and Φ are set at $\varsigma = 5 \times 10^{-15}$ m/s, $\mu = 115(\text{MPam}^{1/2})^{-1}$, $V_m = 0.45$, and $\Phi = 8.5 \times 10^{-2}(\text{GPa})^{-1}$, respectively. This figure reveals that the macroscopic crack growth rate da^*/dt increases with the apparent crack tip stress intensity factor K_{Ia}^*. In particular, the larger the pre-existing inherent surface flaw size, the faster the macroscopic crack growth rate. Moreover, matrix bridging effect becomes noticeable at lower values of K_{Ia}^*. The lowest value of K_{Ia}^*, which is indicated by the arrow, is shifted to a higher value by the matrix bridging effect. This lowest threshold stress intensity factor K_{Iscc}^* is given by Eq. 24 with the equality, i.e.,

$$K_{Iscc}^* = 2\sqrt{V_m J_p/\Phi}. \quad (25)$$

This equation represents the explicit formula of the micromechanically derived lowest threshold stress intensity factor in the case of the Barenblatt cohesive force model. Since the elastic moduli of unidirectional GFRP composite, E_L, E_T, ν_{LT}, ν_{TT}, and G_{LT}, can be formulated using the Young's moduli and the Poisson's ratios of fiber and matrix according to the rules of mixtures [7], Φ in Eq. 25 can be expressed in terms of the Young's moduli and the Poisson's ratios of glass fiber and matrix through Eqs. 17 and 18. Hence, the lowest threshold stress intensity factor K_{Iscc}^* is given by the volume fraction of matrix V_m, the fracture energy of polymeric fibrils J_p, and the Young's moduli and the Poisson's ratios of glass fiber and matrix.

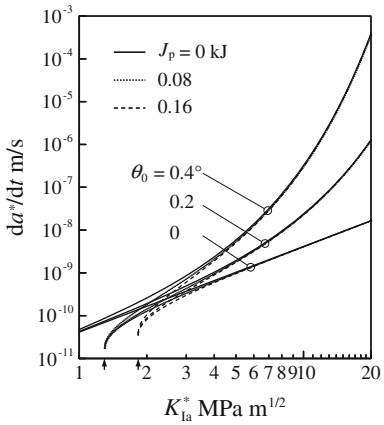

Fig. 5 Macroscopic crack growth rate versus apparent crack tip stress intensity factor due to the remote applied stress

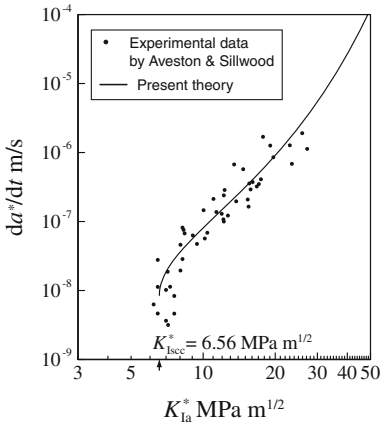

Fig. 6 Comparison between the experimental data of macroscopic crack growth rate and the present theory

Now let us verify by experiment. There is experimental data in the literature [8] on a unidirectional GFRP composite made of E-glass fibers of $V_f = 0.5$ and an orthophthalic polyester resin matrix. Crack propagation experiments were carried out in 1 N sulfuric acid at room temperature. A logarithmic plot of the experimental values of macroscopic crack growth rate versus the apparent crack tip stress intensity factor K_{Ia}^* is shown in Fig. 6. Comparison between experiment and theory is made by setting at $\varsigma = 8.5 \times 10^{-14}$m/s, $\mu = 118(\text{MPam}^{1/2})^{-1}$, $\theta_0 = 0.076°$, $V_m = 0.5$, $J_p = 1.85$ kJ, and $\Phi = 8.6 \times 10^{-2}$ (GPa)$^{-1}$. The prediction of macroscopic crack growth rate is shown by the solid line, and the lowest threshold stress intensity factor is given by $K_{Iscc}^* = 6.56$ MPam$^{1/2}$. The predicted results are consistent with the experimental data. This gives confidence in the used model.

References

1. Sekine H, Miyanaga T (1990) J Soc Mater Sci Jpn 39:1545
2. Sekine H, Beaumont PWR (1998) Compos Sci Technol 58:1659
3. Sekine H, Beaumont PWR (2006) J Mater Sci 41:4604. doi: 10.1007/s10853-006-0328-9

4. Dugdale DS (1960) J Mech Phys Solids 8:100
5. Barenblatt GI (1962) Advances in applied mechanics, 7th edn. Academic, New York
6. Sih GC, Paris PC, Irwin GR (1965) Int J Fract Mech 1:189
7. Jones RM (1975) Mechanics of composite materials. Scripta, Washington
8. Aveston J, Sillwood JM (1982) J Mater Sci 17:3491. doi:10.1007/BF00752194